Heliyon 10 (2024) e38956

Contents lists available at ScienceDirect

Heliyon

journal homepage: www.cell.com/heliyon

Research article

Ag nanoparticles on arginine-cyanoguanidine functionalized magnetic g-C_3N_4: A catalyst for nitroaromatic hydrogenation and regioselective click reactions

Mansoureh Daraie [a,**], Mahmood Tajbakhsh [b,*], Ali Ayati [c], Sara Rashidi [a]

[a] Department of Chemistry, Science and Research Branch, Islamic Azad University, P.O. Box 14515/775, Tehran, Iran
[b] Department of Organic Chemistry, Faculty of Chemistry, University of Mazandaran, Babolsar, Iran
[c] Department of Chemical Engineering, Faculty of Advanced Technologies, Quchan University of Technology, Quchan, Iran

ARTICLE INFO

Keywords:
Carbon nitride
Ag nanoparticles
Click reaction
Catalyst
Reduction of nitroaromatic

ABSTRACT

This study describes the development of a novel hybrid nanocatalyst that was obtained by doping magnetic g-C_3N_4 with Ag nanoparticles and modifying it with arginine and cyanoguanidine (Ag@Fe_3O_4-g-C_3N_4-Arg-CG). Comprehensive characterization of the nanocatalyst using techniques such as FTIR, XRD, SEM, and TGA confirmed its structural and morphological properties. The catalytic efficiency of the synthesized nanostructure was evaluated in two key reactions: the reduction of nitroaromatic compounds and a click reaction for 1,2,3-triazole synthesis. The results demonstrate that Ag@Fe_3O_4-g-C_3N_4-Arg-CG effectively reduced various nitroaromatic compounds to substituted anilines at room temperature using $NaBH_4$ as the reducing agent. Nitrobenzene reduction did not proceed in aprotic solvents such as acetonitrile, CH_2Cl_2, and dimethylformamide, whereas it exhibited a high reaction yield in protic solvents such as ethanol and water. The highest yield (100 %) was observed in water at 50 °C using H_2O solvent. Additionally, the nanohybrid exhibited significant potential for "green" click chemistry by efficiently synthesizing 1,2,3-triazoles under mild conditions, with low catalyst loading. Its magnetic properties facilitated easy recovery, and the catalyst maintained high activity over six cycles, making it suitable for sustainable applications in organic transformations.

1. Introduction

Heterogeneous nanocatalysts have gained significant popularity among synthetic organic chemists over recent decades due to their precision engineering, sustainable design, and development. Compared to homogeneous catalysts, heterogeneous catalysts offer several advantages, including milder reaction conditions, easier separation, prevention of contamination, and recyclability without pre-activation. These benefits have led to the rapid development of this field, where highly active and selective catalysts are being designed to address these challenges [1,2]. Recently, various natural and synthetic polymers have been employed to create desired heterogeneous catalysts. Carbon nitrides, a class of polymers consisting of nitrogen and carbon atoms, enhance chemical, functional, and electrical properties [3]. Among them, graphitic carbon nitride (g-C_3N_4), with its stacked graphene-like structure and high degree

* Corresponding author.
** Corresponding author.
E-mail address: tajbaksh@umz.ac.ir (M. Tajbakhsh).

https://doi.org/10.1016/j.heliyon.2024.e38956
Received 23 June 2024; Received in revised form 20 September 2024; Accepted 3 October 2024
Available online 5 October 2024

of condensation, has attracted considerable attention in catalysis, photocatalysis, and light-emitting devices due to its low cost, non-toxicity, and high stability [4–6]. However, g-C_3N_4 suffers from several drawbacks, including low specific surface area, lack of active sites, weak conjugated stacked structures, and high carrier recombination rates [7–9]. Various strategies have been explored to improve the catalytic performance of g-C_3N_4, including morphology control [10,11], copolymerization [12], metal doping [13,14], and surface modification [10]. Metal doping is particularly effective in enhancing catalytic performance, as g-C_3N_4 has abundant free amino groups in its backbone that can readily bind metal ions [3]. It has been demonstrated that doping g-C_3N_4 with noble metal nanoparticles, such as Pd, Pt, Ag, and Au, increases its surface area, chemical efficiency, and reactivity [15–17]. Among these metals, Ag nanoparticles have garnered significant attention due to their cost-effective synthesis, high surface area, high catalytic activity, stability, conductivity, and biocompatibility [18,19].

The incorporation of Ag nanoparticles onto catalyst surfaces also enhances photocatalytic and antibacterial properties due to the metal's surface plasmon resonance, which reduces charge recombination rates and improves absorption in the visible region of the electromagnetic spectrum [20–23]. One of the key challenges in the catalytic applications of g-C_3N_4-based materials is their separation and reusability, which can be addressed by combining them with magnetic Fe_3O_4 nanoparticles. This combination facilitates easy magnetic separation, enhances catalyst durability, and minimizes aggregation [24–27]. Fe_3O_4 nanoparticles possess numerous hydroxyl groups that can be incorporated into a core-shell structure during further organo-functionalization [28].

A wide range of catalytic strategies have been developed for the selective reduction of nitroaromatic compounds using alternative hydrogen sources and cost-effective catalysts. This reaction is relatively safe and has broad synthetic and biological applications, as it reduces nitroarenes to their corresponding amines [28–30]. Nitroaromatic compounds, which are carcinogenic water pollutants, pose significant environmental risks, damaging living organisms [30,31]. For the catalytic reduction of nitroarenes, metal nanoparticle-doped nanocatalysts combined with $NaBH_4$ as a hydride donor are employed under moderate conditions [30,32,33]. This method is environmentally friendly and has shown promising results in nitroarene reduction.

Triazoles are crucial compounds in both biology and chemistry [34,35]. Sustainable protocols and heterogeneous catalysis have been developed to synthesize these molecules efficiently [36]. 1,2,3-Triazole-bearing N-heterocyclic systems are key structural components of various biologically active compounds, serving as amide bond surrogates [37]. 1,2,3-Triazoles have demonstrated antitubercular [38], antiviral [39], antibacterial, antifungal [40], and anticancer activities [41]. These compounds have been utilized to create several anti-cancer, anti-HIV, and antibacterial drugs through amide-triazole isosteric substitutions [42,43]. Various methods for synthesizing 1,2,3-triazoles have been reported [44,45].

This study aimed to develop an efficient nanocatalyst for organic transformations such as the reduction of nitroaromatic compounds and the synthesis of 1,2,3-triazoles through a click reaction. Ag nanoparticles were synthesized using *Camellia sinensis* leaves as a reducing and stabilizing agent and deposited onto arginine- and cyanoguanidine-modified magnetic g-C_3N_4 to form a hybrid Ag@Fe_3O_4-g-C_3N_4-Arg-CG nanostructure. This hybrid was fully characterized using various techniques, and its catalytic performance was evaluated in two reactions: the reduction of nitroaromatic compounds with $NaBH_4$ and the synthesis of 1,2,3-triazoles via a click reaction. Additionally, the recyclability of the nanocatalyst was tested in both reactions.

2. Experimental section

2.1. Chemicals

All chemicals used for nanocatalyst synthesis and performance evaluation, including melamine ($C_3H_6N_6$, 99 %), iron chlorides ($FeCl_2{\cdot}4H_2O$ and $FeCl_3{\cdot}6H_2O$), arginine, cyanoguanidine (2-cyanoguanidine), ammonium hydroxide solution (NH_4OH, 25 %), triethylamine (TEA), silver nitrate ($AgNO_3$, 99 %), acetonitrile, 1,3,5-triamino-2,4,6-triazine, and nitro-compounds were purchased from Sigma-Aldrich Co. and used as received. Green tea leaves (*Camellia sinensis*) were collected from Lahijan city, Gilan province, Iran. All methods involving plants and their materials conformed to relevant institutional, national, and international guidelines. Tea is a common and non-endangered plant in Iran.

2.2. Catalyst synthesis

2.2.1. Synthesis of magnetic g-C_3N_4

g-C_3N_4 nanosheets were synthesized by thermally polycondensing 1,3,5-triamino-2,4,6-triazine in a semi-closed ceramic crucible at 530 °C in air at a rate of 5 °C/min for 5 h. The product was cooled, washed, and ground in an agate mortar. To synthesize magnetic g-C_3N_4, the g-C_3N_4 (15 g) was dispersed in water (140 mL), followed by the addition of $FeCl_3{\cdot}6H_2O$ (1.37 g) and $FeCl_2{\cdot}4H_2O$ (0.5 g). After heating to 60 °C, NH_4OH solution (11 mL, 25 %) was added, and the mixture was stirred for 60 min. The magnetic Fe_3O_4-g-C_3N_4 nanostructure was magnetically separated, washed with water, and dried at room temperature.

2.2.2. Synthesis of Fe_3O_4-g-C_3N_4-Arg-CG

Fe_3O_4-g-C_3N_4 (1.2 g) was dispersed in water (100 mL), and arginine (0.7 g) and triethylamine (0.7 g) were added. The mixture was stirred and refluxed overnight, then separated magnetically and washed with water-ethanol solutions (3:1). The product was dispersed in water (50 mL), followed by the addition of dicyandiamide (0.34 g) and diluted hydrochloric acid (5 mL, 5 %), and refluxed at 100 °C for 6 h. The precipitate was magnetically separated, washed with ethanol solution (50 %), and dried at ambient temperature.

2.2.3. Synthesis of Ag@Fe_3O_4-g-C_3N_4-Arg-CG

Ag nanoparticles (Ag NPs) were synthesized using *Camellia sinensis* leaves extract as a reducing agent [46]. Fresh leaves were collected, dried, and extracted in distilled water using Soxhlet. The extract was stored at 5 °C. Fe_3O_4-g-C_3N_4-Arg-CG (300 mg) was dispersed in an $AgNO_3$ solution (50 mL, 1.5 mM), and *Camellia sinensis* extract (10 mL, 2 %) was added. The mixture was stirred at 60 °C for 2 h, and the product was magnetically separated, washed with ethanol/water, and dried. Inductively coupled plasma (ICP) analysis estimated the Ag content at ~0.4 wt%. The entire synthesis procedure is shown in Scheme 1.

2.3. Catalytic reduction of nitroaromatic compounds

The catalytic performance of Ag@Fe_3O_4-g-C_3N_4-Arg-CG was evaluated using the reduction of nitrobenzene, as depicted in Scheme 2. In a 50 mL borosilicate glass tube, 0.02 g of catalyst was added to a solution of 123 mg nitrobenzene (1 mmol) in 5 mL water. A freshly prepared $NaBH_4$ solution (0.5 mM) was then added to the mixture under vigorous stirring. The reaction was heated to 50 °C and monitored using thin-layer chromatography (TLC) with ethyl acetate (10 %) in hexane. After the reaction, the catalyst was magnetically separated, and the solvent was evaporated to isolate the hydrogenated product. The catalyst was rinsed with 30 mL ethanol (EtOH) and dried overnight at 50 °C, after which it was collected and reused for subsequent reactions.

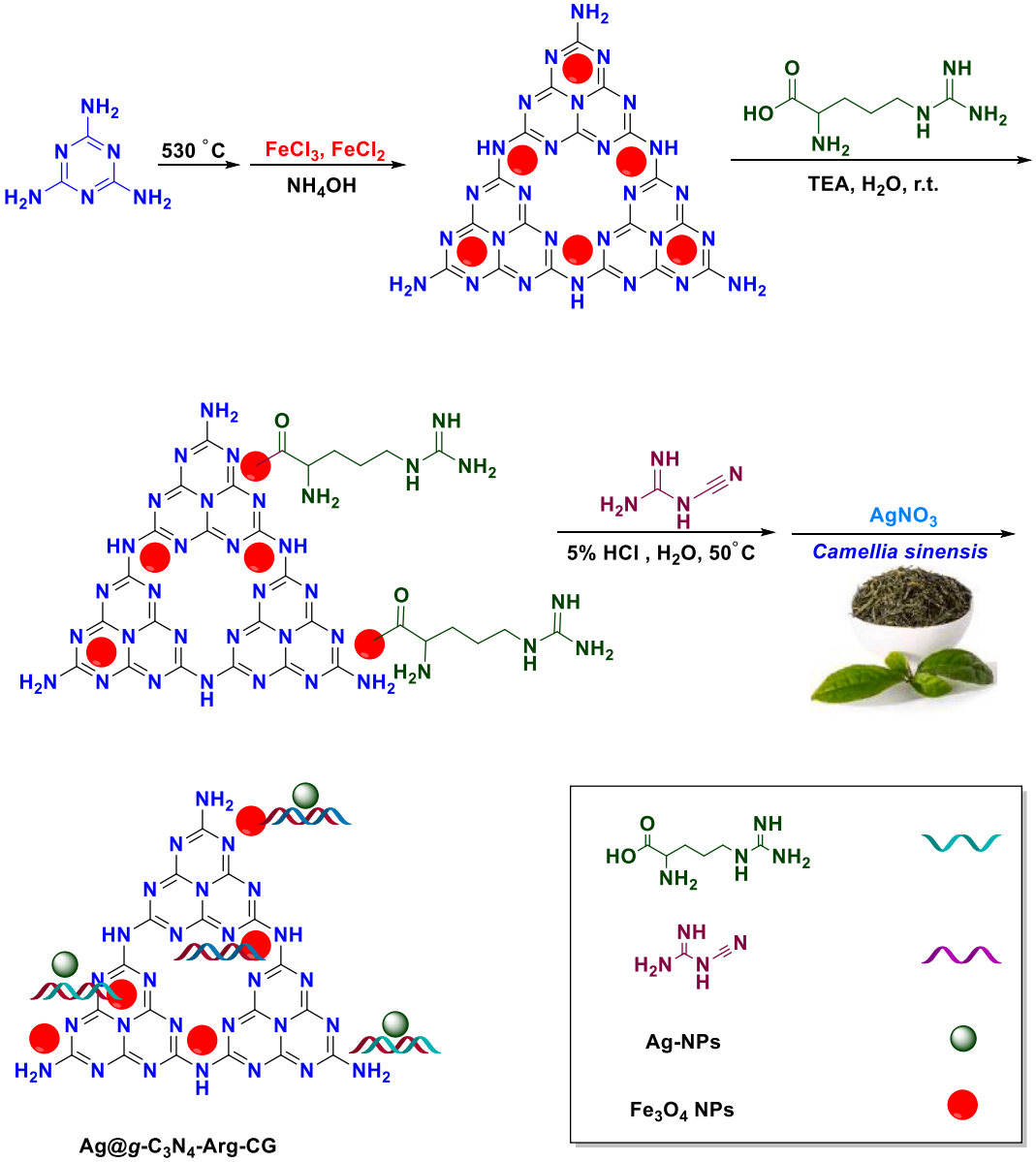

Scheme 1. The schematic route of Ag@Fe_3O_4-g-C_3N_4-Arg-CG preparation.

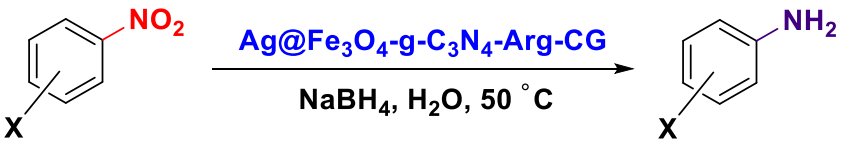

Scheme 2. The reaction of nitrobenzene reduction.

The generality of this protocol was assessed in the reduction of nitroaromatic compounds using Ag@Fe_3O_4-g-C_3N_4-Arg-CG. Different catalyst dosages were added to 5 mL of aqueous solution containing 0.001 mol nitroaromatic compounds. The mixture was stirred vigorously at room temperature, followed by the addition of 2 mmol $NaBH_4$. The reaction was heated to 50 °C, and upon completion, confirmed by TLC, the catalyst was separated, and the product was purified by recrystallization.

2.4. Synthesis of 1,4-disubstituted 1,2,3-triazoles

Ag@Fe_3O_4-g-C_3N_4-Arg-CG was also employed in the catalytic synthesis of 1,4-disubstituted 1,2,3-triazoles via a click reaction. In this reaction, 0.02 g of the nanocatalyst was added to a solution containing an alkyl halide or α-haloketone (1 mmol), a terminal alkyne (1 mmol), and sodium azide (1.2 mmol) in 5 mL of water. The reaction mixture was stirred at room temperature until completion. The solid residue was filtered and recrystallized from ethanol to obtain the pure product (Scheme 3).

2.5. Material characterization

The successful synthesis of the nanocatalyst was confirmed using Fourier-transform infrared (FTIR) spectroscopy with a PERKIN-ELMER Spectrum. The phase and crystallinity of the nanocatalyst were identified using X-ray powder diffraction (XRD) with Cu Kα radiation (wavelength 1.78897 Å, 40 mA, and 40 keV). Scanning electron microscopy (SEM) images were obtained with a FESEM-TESCAN MIRA3 microscope equipped with energy dispersive X-ray (EDX) for elemental analysis. Transmission electron microscopy (TEM) images were captured using a Philips CM120 microscope at 100 kV. Inductively coupled plasma atomic emission spectroscopy (ICP-AES) analysis was performed using a Vista-Pro Varian analyzer to estimate the amount of Ag nanoparticles on the catalyst surface. The thermal stability of the catalyst was analyzed with an SDT-Q600 simultaneous TGA instrument (TA Instruments) under an Ar atmosphere.

3. Results and discussion

3.1. Nanocatalyst characterization

To confirm the formation of the Ag@Fe_3O_4-g-C_3N_4-Arg-CG nanocatalyst, its FTIR spectrum was recorded and compared with those of magnetite, g-C_3N_4, and Fe_3O_4-g-C_3N_4-Arg-CG, as shown in Fig. 1. In the FTIR spectrum of Fe_3O_4 nanoparticles, the absorption band at 590 cm^{-1} is attributed to the trivalent Fe–O tetrahedral structure [47,48], while the broad band at 3445 cm^{-1} corresponds to hydroxyl groups on the surface of Fe_3O_4. The g-C_3N_4 spectrum displays several characteristic bands: (i) 808 cm^{-1} related to triazine ring bending vibrations, (ii) 1240–1408 cm^{-1} associated with C–N stretching vibrations [49], (iii) 1648 cm^{-1} corresponding to C=N stretching vibrations, and (iv) 3422 cm^{-1} attributed to NH bending.

The spectrum of Fe_3O_4-g-C_3N_4-Arg confirms the presence of L-arginine on the surface of g-C_3N_4 nanoplates through C=O (1708 cm^{-1}) and C–O (1215–1322 cm^{-1}) stretching vibrations. These are further supported by the presence of N–H and C–H bonds in the modified g-C_3N_4 nanosheets. All these peaks are observed in the FTIR spectrum of the Ag@Fe_3O_4-g-C_3N_4-Arg-CG structure, with minor shifts compared to those of the individual components (see Fig. 1), confirming the successful fabrication of the catalyst. A weak band at 2960 cm^{-1} is attributed to aliphatic C–H stretching vibrations, while the stretching vibrations of the alkyl and ester groups of the arginine moiety appear at 2850–2900 cm^{-1} and 1730 cm^{-1}, respectively [50]. The presence of Ag NPs did not significantly affect the FTIR spectrum, indicating the stability of the nanocomposite despite the deposition of Ag NPs on its surface.

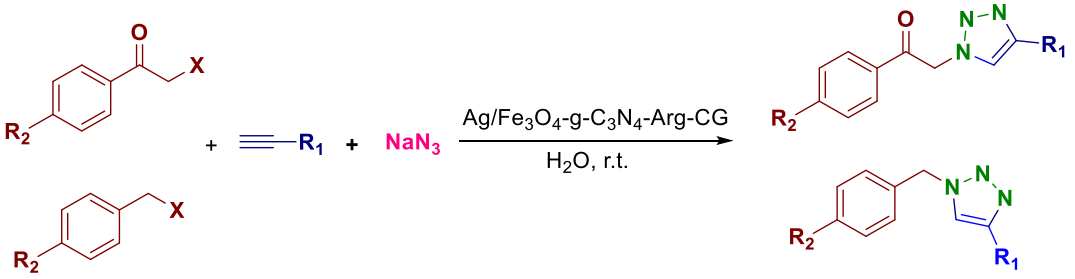

Scheme 3. Detailed schematic of a 1,4-disubstituted 1,2,3-triazole synthesis reaction.

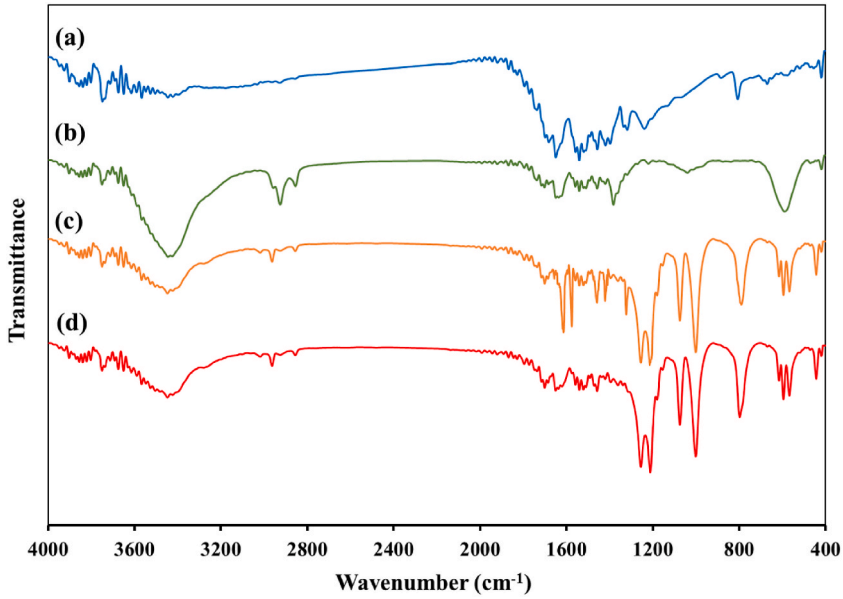

Fig. 1. FTIR spectra of a) g-C_3N_4, b) Fe_3O_4, c) Fe_3O_4-g-C_3N_4-Arg-CG, and Ag@Fe_3O_4-g-C_3N_4-Arg-CG.

Fig. 2 shows the XRD patterns of the synthesized g-C_3N_4, magnetic g-C_3N_4, and Ag@ Fe_3O_4- g-C_3N_4-Arg-CG nanostructures in the 2θ range of 10–80°. The peaks at 2θ = 31.1°, 36.4°, 44.1°, 54.3°, 57.6°, and 62.8° correspond to the face-centered cubic structure of Fe_3O_4 nanoparticles, attributed to the (220), (311), (400), (422), (511), and (440) planes, respectively [51] (JCPDS card no. 19–0629). The peak at 44.4° is assigned to the (200) plane of Ag nanoparticles, confirming their successful incorporation into the composite. In addition, the small peak at 2θ = 27.6° is characteristic of g-C_3N_4, confirming its presence in the structure. The overall XRD pattern demonstrates the successful integration of Fe_3O_4, Ag NPs, g-C_3N_4, and L-arginine. The absence of significant peak shifts indicates that the structural integrity of these components is maintained. The arginine and cyanoguanidine groups do not show distinct diffraction peaks in the XRD patterns due to their amorphous nature, but their incorporation is confirmed by complementary techniques like FTIR.

The morphology of the Ag@Fe_3O_4-g-C_3N_4-Arg-CG nanocatalyst was investigated using FE-SEM, as shown in Fig. 3a. Slight aggregation of spherical nanoparticles, with an average size of 28 nm, is visible on the surface, likely due to Fe_3O_4 and Ag NPs covering the g-C_3N_4 substrate. For a more detailed analysis, the nanocatalyst's morphology was further examined via TEM. The TEM images in

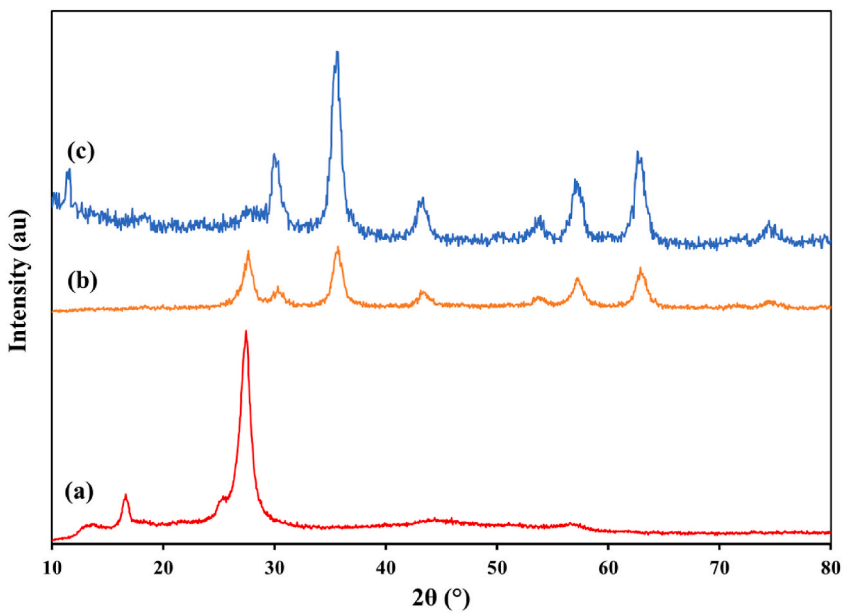

Fig. 2. XRD pattern of a) g-C_3N_4, b) Fe_3O_4-g-C_3N_4, c) Ag@Fe_3O_4-g-C_3N_4-Arg-CG.

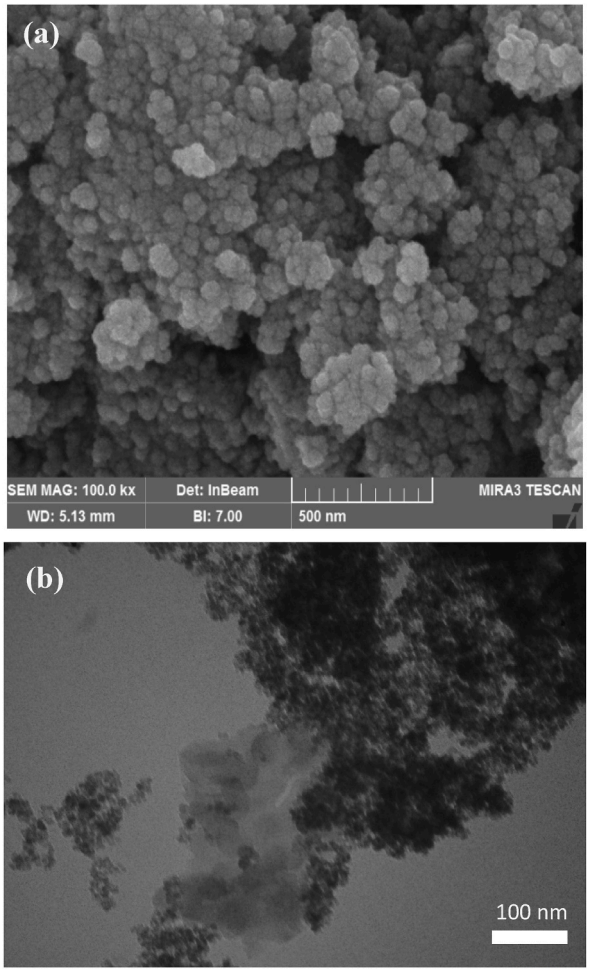

Fig. 3. The (a) SEM, and (b) TEM images of prepared Ag@Fe_3O_4-g-C_3N_4-Arg-CG nanomaterials.

Fig. 3b clearly show the presence of g-C_3N_4 nanosheets, along with Fe_3O_4 and Ag NPs distributed across the structure.

Elemental dot-mapping analyses were also conducted to identify the elements present and their distribution within the nanocatalyst structure. The results of the EDX and elemental dot-mapping analysis are shown in Fig. 4. According to the EDX data, the quantities of the elements in Ag@Fe_3O_4-g-C_3N_4-Arg-CG are consistent with the amounts used during synthesis. The uniform distribution of Fe and Ag nanoparticles on g-C_3N_4 indicates that Fe_3O_4 and Ag NPs are evenly dispersed across the material's surface.

TGA analysis of the synthesized Ag@Fe_3O_4-g-C_3N_4-Arg-CG nanostructure was carried out between 25 and 800 °C to assess its thermal stability (Fig. 5). The analysis revealed three significant weight loss stages. The first, a minor weight loss of less than 2 %, occurred around 30–120 °C and was attributed to the evaporation of adsorbed water. The second weight loss, approximately 20 %, took place between 290 and 355 °C, likely due to the decomposition of arginine and biguanide substituents attached to the g-C_3N_4 substrate. The major weight loss, around 40 %, was observed between 450 and 600 °C, corresponding to the degradation of the g-C_3N_4 structure. This thermal profile indicates that the prepared nanostructure is suitable for various applications, including catalysis, sensing, and adsorption.

3.2. Catalytic study

3.2.1. Nitroaromatic reduction

The catalytic activity of Ag@Fe_3O_4-g-C_3N_4-Arg-CG was investigated for the reduction of nitroaromatic compounds, with nitrobenzene reduction chosen as a model reaction to optimize the reaction conditions. The effects of temperature, catalyst dosage, reaction time, and solvent type (protic and aprotic) were thoroughly studied, and the results are summarized in Table 1. As the results (entries 1–4) show, nitrobenzene reduction did not proceed well in the absence of catalysts, demonstrating the importance of catalysts in this reaction.

The catalyst dosage was varied from 0.01 g to 0.03 g to determine its impact on the reaction efficiency. As shown in Table 1, the optimal catalyst amount was 0.02 g, which gave the highest yield (100 %) when used in H_2O at 50 °C (entry 10). A lower catalyst

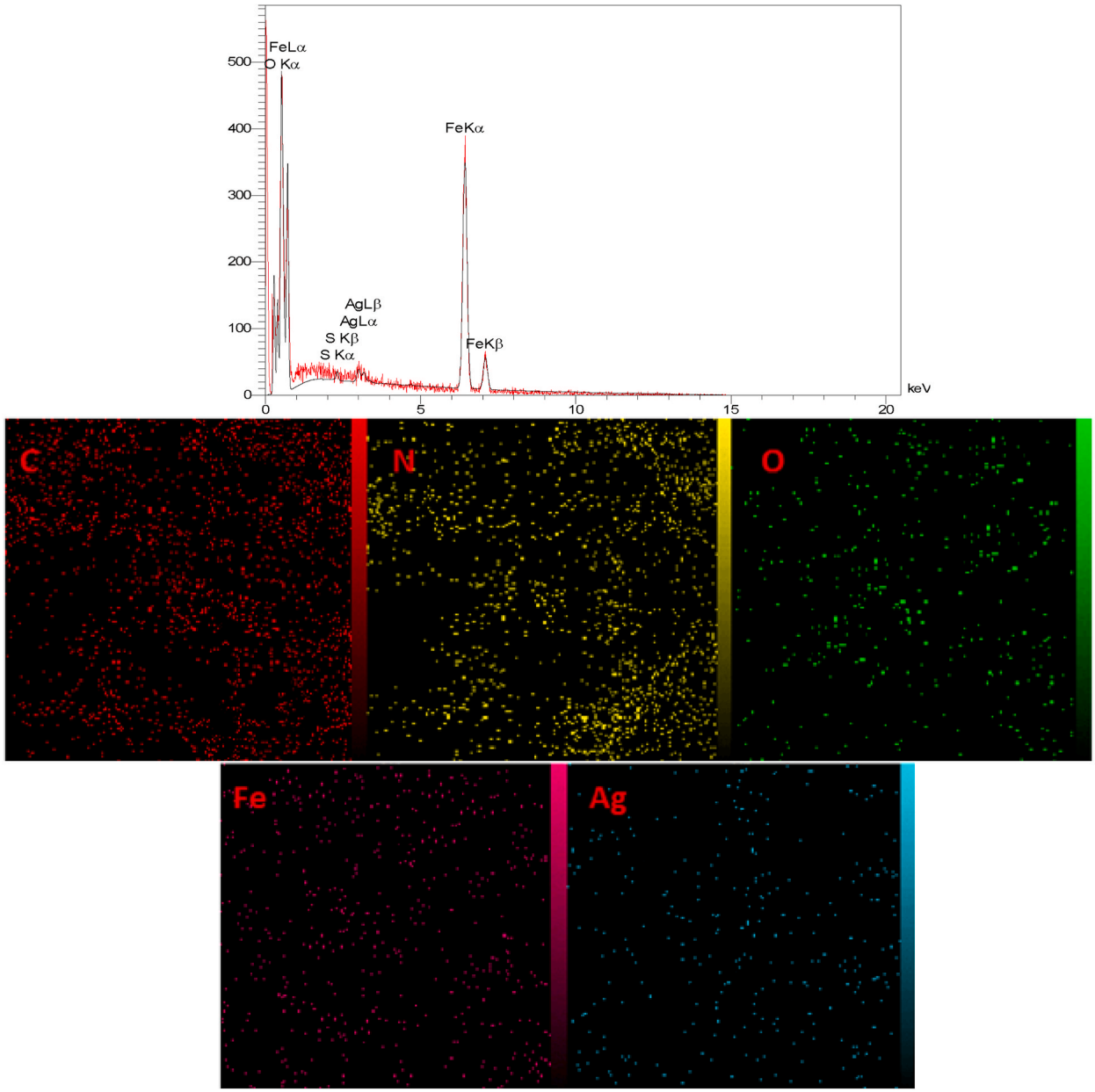

Fig. 4. EDX and elemental dot-mapping analysis of Ag@Fe_3O_4-g-C_3N_4-Arg-CG nanostructure.

dosage of 0.01 g resulted in a slightly reduced yield of 95 % (entry 13), whereas increasing the dosage to 0.03 g (entry 14) did not improve the yield beyond 100 %. At lower catalyst dosages, fewer active sites are available for the reduction reaction, leading to a decrease in reaction efficiency. Temperature also played a significant role in the reaction yield. Temperature influences both the reaction kinetics and the stability of the catalyst. Reactions performed at room temperature (Table 1, entry 9) showed only moderate yield (45 %), indicating insufficient energy for efficient catalysis. As the temperature increased to 50 °C (entry 10), the yield reached 100 %, suggesting that this temperature is optimal for promoting the reduction reaction. Increasing the temperature to 50 °C enhances the reaction rate by providing more thermal energy, allowing for faster reduction and improved yields. Further increases in temperature, such as 70 °C (entry 11) and reflux conditions (entry 12), resulted in lower yields (70 % and 85 %, respectively). This suggests that excessive temperatures may destabilize the catalyst or lead to undesired side reactions, highlighting 50 °C as the optimal condition for this reaction. At these higher temperatures, the Ag nanoparticles could experience sintering (aggregation of nanoparticles), which reduces the active surface area, thus diminishing the catalytic efficiency. Additionally, side reactions could become more prominent at elevated temperatures, further reducing the yield.

The time required to achieve maximum yield was also evaluated. The optimal reaction time was found to be 30 min (entries 6, 9,

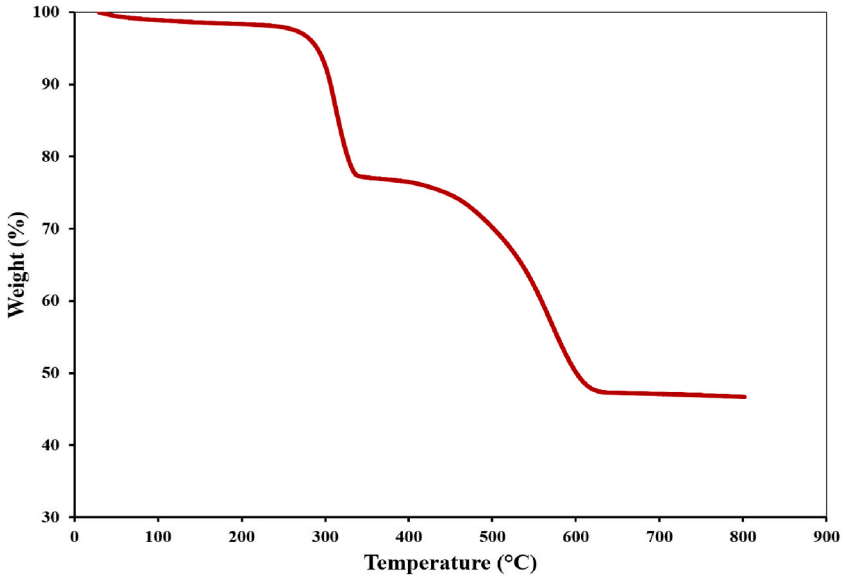

Fig. 5. The TGA curve of Ag@Fe_3O_4-g-C_3N_4-Arg-CG.

Table 1
Optimization conditions for nitrobenzene reduction.

Entry	Catalyst amount (g)	Solvent	Temperature (°C)	Time (min)	Yield (%)[a]
1	–	EtOH	50	60	12
2	–	CH_3CN	50	60	10
3	–	CH_2Cl_2	under reflux	60	trace
4	–	H_2O	50	60	15
5	0.02	EtOH	50	30	70
6	0.02	CH_3CN	50	40	10
7	0.02	DMF	50	40	10
8	0.02	CH_2Cl_2	under reflux	45	8
9	0.02	H_2O	room temperature	45	45
10	0.02	H_2O	50	30	100
11	0.02	H_2O	70	35	70
12	0.02	H_2O	under reflux	30	85
13	0.01	H_2O	50	30	95
14	0.03	H_2O	50	30	100

a: Rection conditions, 0.02 g of Ag@Fe_3O_4-g-C_3N_4-Arg-CG, H_2O (5 mL), $NaBH_4$ (0.5 mM), 50 °C.
b: Yields refer to isolated products.

10), with a yield of 100 % achieved at this duration. Longer reaction times, such as 40 or 45 min (entries 2, 3, 4, 7), either did not improve or even reduced the yield. Once the reaction reaches completion, extending the reaction time does not provide additional benefits and may actually result in side reactions or catalyst deactivation, leading to lower yields. The decline in yield with prolonged reaction times at higher temperatures (e.g., entries 7 and 8) can be attributed to the gradual degradation of the catalyst or the formation of by-products. This emphasizes that the optimal time of 30 min is sufficient to achieve maximum conversion without compromising the catalyst or producing side reactions.

Solvent choice had a significant effect on the yield of the reaction. As the results show, nitrobenzene reduction did not proceed in aprotic solvents such as acetonitrile, CH_2Cl_2, and DMF (Table 1, entries 6–8), whereas it gave a high aniline yield in protic solvents such as ethanol and water (Table 1, entries 9–14). The highest yield (100 %) was observed in water at 50 °C using H_2O solvent (Table 1, entries 10 and 14), while aprotic solvents resulted in little to no product formation (entries 6–8). It can be attributed to the role of solvents in proton transfer, which is essential in reducing nitro groups to amines. Protic solvents like ethanol and water can donate protons, facilitating the reduction reaction by stabilizing reaction intermediates and enhancing the proton transfer required for nitrobenzene reduction. H_2O, in particular, is highly polar, and its ability to stabilize charged species and intermediates makes it an excellent solvent for catalytic reactions involving electron and proton transfer. In contrast, aprotic solvents lack the ability to donate protons, which impedes the reduction process and results in low yields. Additionally, protic solvents are better at interacting with the catalyst (Ag@Fe_3O_4-g-C_3N_4-Arg-CG), enhancing the efficiency of the reaction through improved solubility of reactants and better catalyst-solvent interactions. The results indicated that using 0.02 g of Ag@Fe_3O_4-g-C_3N_4-Arg-CG nanocatalyst in H_2O solvent at 50 °C for 30 min (Table 1, entry 10, optimal conditions) achieved the highest aniline yield.

The substituents on the nitrophenol ring can significantly affect the rate and efficiency of the catalytic reduction to aminophenol. We validated the proposed protocol by utilizing the Ag@Fe_3O_4-g-C_3N_4-Arg-CG nanocatalyst to reduce different nitroaromatic compounds, which acted as starting materials, resulting in the production of various aromatic amines. Table 2 presents the obtained results. The nanocatalysts demonstrate excellent performance in reducing the chosen substrates, resulting in high efficiencies (~100 %) within short reaction times. Electron-withdrawing groups (e.g., halogens, nitro groups) tend to increase the electrophilicity of the nitro group, making the reduction process easier and faster as they facilitate the interaction of nitrophenol with the hydride ions on the Ag NP surface. In contrast, electron-donating groups (e.g., alkyl or hydroxyl groups) reduce the electrophilicity of the nitro group, thereby hindering the reduction reaction and lowering the conversion rate. The position of the substituents also plays a role: ortho- and para-substituted nitrophenols tend to undergo reduction more readily due to their proximity to the nitro group, whereas meta-substituted nitrophenols often show slower reaction rates due to steric hindrance and electronic effects. These variations underscore the importance of understanding the electronic environment of the substrate when designing catalytic systems for nitroaromatic reductions. The catalytic activity of Ag@Fe_3O_4-g-C_3N_4-Arg-CG nanohybrid is likely influenced by these factors, with certain substituents enhancing or inhibiting the adsorption and electron transfer processes on the Ag nanoparticle surface.

3.2.2. *Reaction mechanism*

The catalytic reduction mechanism of 4-nitrophenol to 4-aminophenol using Ag@Fe_3O_4-g-C_3N_4-Arg-CG nanohybrid is shown in Fig. 6 [52,53]. In this reaction, NaBH4 serves as the reducing agent, generating hydride ions (H^-) that adsorb onto the nanocatalyst's surface. These hydride ions are subsequently transferred to the Ag nanoparticles (Ag NPs), where the reduction process takes place. The 4-nitrophenol substrate approaches and adsorbs onto the Ag NPs surface, following the principles of the Langmuir isotherm, which suggests that the adsorption of both hydride ions and 4-nitrophenol is reversible on the Ag surface. At the catalyst-substrate interface, electron transfer occurs between the Ag@Fe_3O_4-g-C_3N_4-Arg-CG nanohybrid and 4-nitrophenol. The rate of electron transfer is directly related to the overall conversion rate of the reaction. Several reaction intermediates, including nitrosophenol and hydroxylaminophenol, are formed before the final product, 4-aminophenol, is generated, as illustrated in Fig. 6. After product formation, the

Table 2
Reduction of aromatic nitro compounds in the presence of Ag@Fe_3O_4-g-C_3N_4-Arg-CG.[a]

Entry	Product	Time (min)	Yield (%)[b]	Melting point (Abs./Lit.) [30]
1	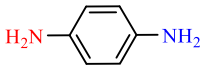	30	100	142-145/141-143
2	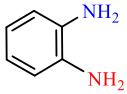	38	98	102-103/102-104
3	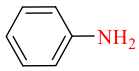	35	100	Liquid
4	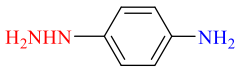	65	97	Oil
5	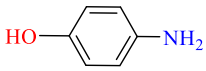	55	95	185-188/187
6	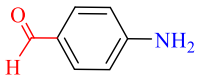	35	100	76-77/78
7	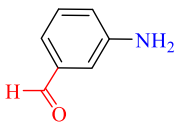	40	100	28-30/29-30
8	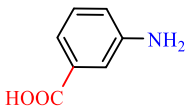	120	97	181-182/180
9	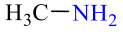	45	98	Liquid

[a] Reaction conditions, 0.02 g of Ag@Fe_3O_4-g-C_3N_4-Arg-CG, H_2O (5 mL), $NaBH_4$ (0.5 mM), 50 °C.
[b] Yields refer to isolated products.

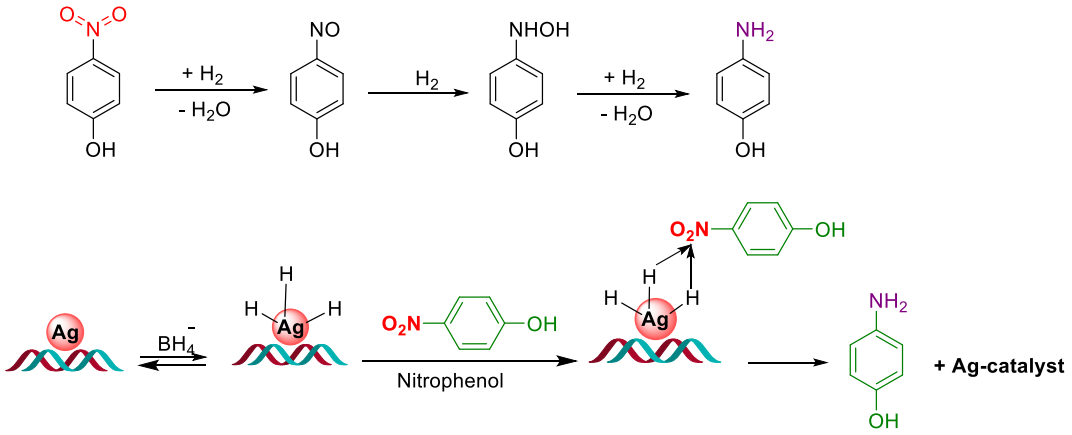

Fig. 6. The plausible mechanism for the reduction of nitrophenol on the Ag@Fe_3O_4-g-C_3N_4-Arg-CG nanocatalyst.

aminophenol desorbs from the catalyst surface, freeing up active sites for the next reaction cycle. The diffusion of reactants over the Ag NPs occurs efficiently, and the system quickly establishes an adsorption/desorption equilibrium, facilitating rapid turnover. Based on the reaction mechanism, it can be proposed that the rate-determining step is the interaction between the adsorbed hydride ions and 4-nitrophenol on the Ag NPs surfaces. This step is critical for initiating the reduction and governs the overall reaction rate.

3.2.3. Click reaction for the synthesis of 1,2,3-triazoles

The catalytic activity of the Ag@Fe_3O_4-g-C_3N_4-Arg-CG nanohybrid was evaluated in the click reaction for the synthesis of 1,2,3-triazoles. To optimize the reaction conditions, a mixture of phenacyl bromide (1 mmol), phenylacetylene (1 mmol), and sodium azide (1.1 mmol) was used as a model reaction. Various temperatures, solvents, and catalyst amounts were tested. The optimization results are summarized in Table 3. As shown in Table 3, the best results were achieved in water, which is an ideal solvent for green chemistry applications.

A variety of substrates with varying electron densities were used for the reaction and different 1,2,3-triazoles were produced (Table 4). These results demonstrate the efficiency of Ag@Fe_3O_4-g-C_3N_4-Arg-CG as an effective catalyst for a wide variety of substrate reactions, with a fast and high-yielding reaction to corresponding 1,2,3-triazoles.

3.2.4. Plausible mechanism of 1,2,3-triazoles synthesis

The reaction mechanism can be proposed similarly to that of 1,4-disubstituted 1,2,3-triazole synthesis using a copper(I)-catalyzed azide-alkyne cyclo-addition reaction [57]. Fig. 7 illustrates the proposed mechanism of the current Ag-catalyzed azide-alkyne click reaction. The plausible mechanism starts with the generation of silver acetylide I. Based on density functional theory calculations, stepwise additions (β-1, β-2, β-3) are preferred to concerted cycloadditions (β-direct), leading to the five-membered Ag-contained intermediate IV. Finally, intermediate IV results 1,2,3-triazole.'

3.2.5. Hot filtration

To investigate the nature of the heterogeneous catalyst, a hot filtration test was performed. In true heterogeneous catalysis, the catalyst remains immobilized on the support. Alternatively, the catalytic species could leach into the reaction medium and then redeposit on the support. Following the standard protocol, Ag@Fe_3O_4-g-C_3N_4-Arg-CG was removed from the reaction mixture after 15 min, and the reaction was monitored to see if it continued in the absence of the catalyst. As shown in Fig. 8, after the removal of Ag@Fe_3O_4-g-C_3N_4-Arg-CG, no further progress was observed, and the reaction yield remained unchanged, confirming that the catalysis was indeed heterogeneous.

Table 3
Optimization conditions for the synthesis of 1,2,3-triazoles using Ag@Fe_3O_4-g-C_3N_4-Arg-CG

Entry	Catalyst amount (g)	Solvent	Temperature	Time (min)	Yield (%)
1	0.03	EtOH	under reflux	35	94
2	0.03	CH_3CN	under reflux	40	89
3	0.03	CH_2Cl_2	under reflux	40	75
4	0.03	H_2O	room temperature	25	94
5	0.03	H_2O	50 °C	35	90
6	0.03	H_2O	under reflux	10	98
7	0.02	H_2O	under reflux	20	95
8	0.03	H_2O	under reflux	10	98

Table 4
Synthesis of 1,2,3-triazole derivatives using Ag@Fe_3O_4-g-C_3N_4-Arg-CG [54–56].

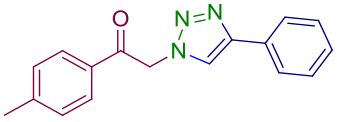	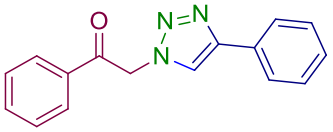	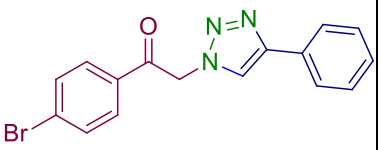
4a, M. P.= 159-161 12 min, 97 %	4b, M. P.= 167-169 10 min, 98%	4c, M. P.= 116-117 14 min, 96%
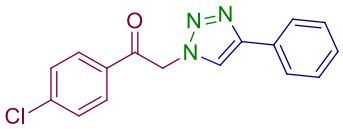	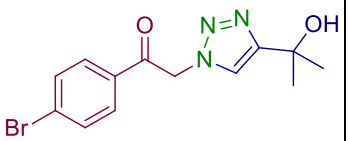	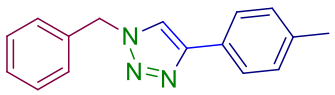
4d, M. P.= 111-112 12 min, 96%	4e, M. P.= 153-154 20 min, 94%	4f, M. P.= 146-149 15 min, 95%
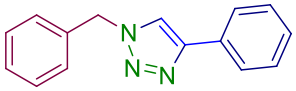	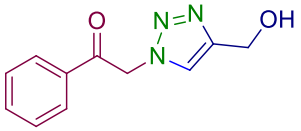	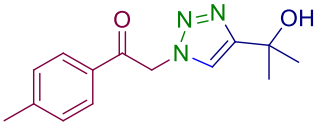
4g, M. P.= 125-127 18 min, 94%	4h, M. P.= 110-113 20 min, 95%	4i, M. P.= 165-168 18 min, 93%
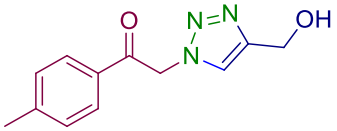	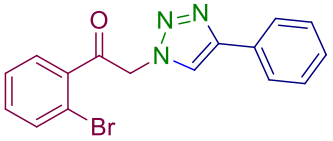	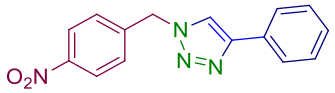
4j, M. P.= 183-185 20 min, 91%	4k, M. P.= 189-191 18 min, 94%	4l, M. P.= 154-155 12 min, 95%
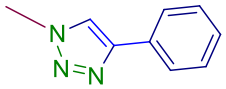	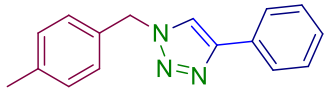	
4m, CH_3I, M. P.= 123-125 25 min, 90%	4n, M. P.= 106-108 17 min, 92%	

3.3. Catalyst recyclability

We conducted a study on the stability/reusability of the Ag@Fe_3O_4-g-C_3N_4-Arg-CG catalyst for six consecutive cycles, considering its importance for large-scale applications. This was accomplished by separating the nanocatalyst after the reaction was complete, rinsing it with ethanol and water, drying it in a vacuum, and then reusing it in a subsequent run under the same reaction conditions. The results are shown in Fig. 9. As shown, the catalytic yields of the nitrobenzene reduction and click reaction only showed reductions of 8 % and 11 %, respectively after six runs. The results demonstrate the high recyclability of the Ag@Fe_3O_4-g-C_3N_4-Arg-CG

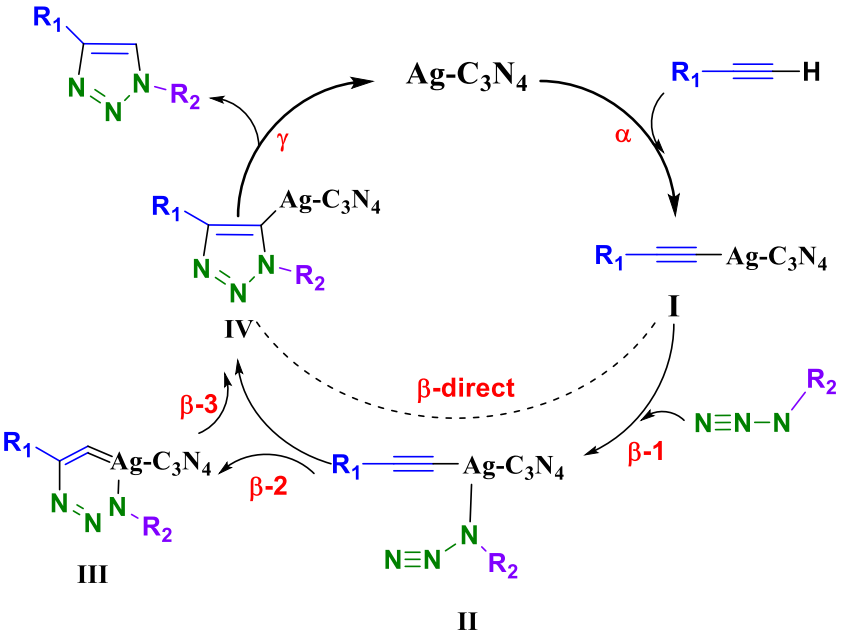

Fig. 7. Plausible mechanism of 1,2,3-triazoles synthesis using Ag@Fe_3O_4-g-C_3N_4-Arg-CG.

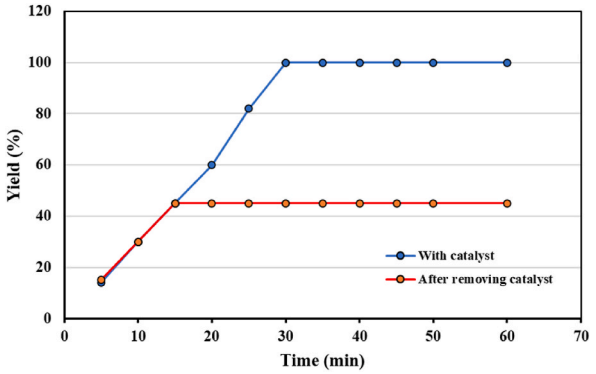

Fig. 8. Hot filtration test for the reduction of nitro aromatic compound.

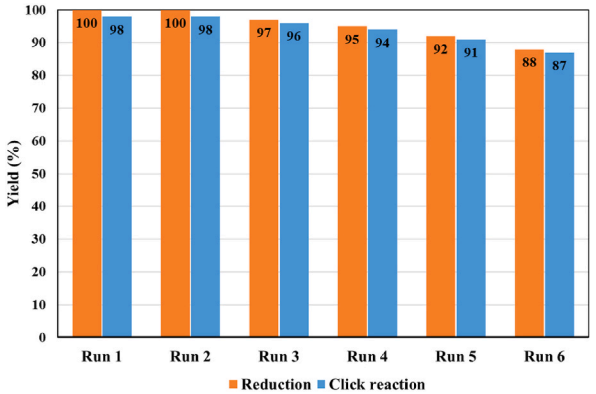

Fig. 9. The recyclability of Ag@Fe_3O_4-g-C_3N_4-Arg-CG nanocatalyst in different reactions.

nanocatalyst.

4. Conclusions

The Ag@Fe_3O_4-g-C_3N_4-Arg-CG nanocatalyst represents a significant advancement in catalytic systems for organic transformations. This study demonstrated that the hybrid nanocatalyst exhibited remarkable efficiency in two key reactions: the reduction of nitroaromatic compounds to substituted anilines and the synthesis of 1,2,3-triazoles through click chemistry. Notably, the reduction process achieved high yields in aqueous media at room temperature, with water as the optimal solvent. The catalyst's ability to facilitate the reduction of a diverse range of nitroaromatic substrates highlights its versatility and effectiveness. Additionally, the successful synthesis of 1,2,3-triazoles under mild conditions with low catalyst loading illustrates its potential for green chemistry applications. The magnetic properties of the nanocatalyst allowed for straightforward recovery and reuse, with minimal loss in catalytic performance over six cycles, demonstrating excellent stability and reusability. Overall, the Ag@Fe_3O_4-g-C_3N_4-Arg-CG nanocatalyst not only addresses the challenges associated with traditional catalytic systems but also paves the way for sustainable and efficient processes in both academic and industrial settings. Its multifunctional activity and adaptability make it a valuable addition to the field of heterogeneous catalysis.

Data availability

The raw/processed data that supports the findings of this study is available from the corresponding author upon reasonable request.

CRediT authorship contribution statement

Mansoureh Daraie: Writing – review & editing, Methodology, Investigation, Funding acquisition, Conceptualization. **Mahmood Tajbakhsh:** Writing – review & editing, Supervision, Methodology, Funding acquisition. **Ali Ayati:** Writing – original draft, Methodology. **Sara Rashidi:** Methodology, Investigation.

Declaration of competing interest

The authors declare that they have no known competing financial interests or personal relationships that could have appeared to influence the work reported in this paper.

Acknowledgements

M. Tajbakhsh & M. Daraie are grateful to Iran National Science Foundation (INSF) for financial support provided by project (4016139). We also appreciate Mazandaran University Research Council for their help and supports.

References

[1] A.I. Osman, A. Ayati, P. Krivoshapkin, B. Tanhaei, M. Farghali, P.-S. Yap, A. Abdelhaleem, Coordination-driven innovations in low-energy catalytic processes: advancing sustainability in chemical production, Coord. Chem. Rev. 514 (2024) 215900, https://doi.org/10.1016/j.ccr.2024.215900.
[2] A.I. Osman, A.M. Elgarahy, A.S. Eltaweil, E.M. Abd El-Monaem, H.G. El-Aqapa, Y. Park, Y. Hwang, A. Ayati, M. Farghali, I. Ihara, A.a.H. Al-Muhtaseb, D. W. Rooney, P.-S. Yap, M. Sillanpää, Biofuel production, hydrogen production and water remediation by photocatalysis, biocatalysis and electrocatalysis, Environ. Chem. Lett. (2023), https://doi.org/10.1007/s10311-023-01581-7.
[3] M. Heydari, N. Azizi, Z. Mirjafari, M.M. Hashemi, Aluminum anchored on g-C_3N_4 as robust catalysts for Mannich reaction at ambient temperature, J. Mol. Struct. 1259 (2022) 132731, https://doi.org/10.1016/j.molstruc.2022.132731.
[4] O. Iqbal, H. Ali, N. Li, A.I. Al-Sulami, K. F Alshammari, H.S.M. Abd-Rabboh, Y. Al-Hadeethi, I.U. Din, A.I. Alharthi, R. Altamimi, A. Zada, Z. Wang, A. Hayat, M. Zahid Ansari, A review on the synthesis, properties, and characterizations of graphitic carbon nitride (g-C_3N_4) for energy conversion and storage applications, Mater. Today Phys. 34 (2023) 101080, https://doi.org/10.1016/j.mtphys.2023.101080.
[5] J. Xing, N. Wang, X. Li, J. Wang, M. Taiwaikuli, X. Huang, T. Wang, L. Zhou, H. Hao, Synthesis and modifications of g-C_3N_4-based materials and their applications in wastewater pollutants removal, J. Environ. Chem. Eng. 10 (6) (2022) 108782, https://doi.org/10.1016/j.jece.2022.108782.
[6] Z. Huang, M. Shen, J. Liu, J. Ye, T. Asefa, Facile synthesis of an effective g-C_3N_4-based catalyst for advanced oxidation processes and degradation of organic compounds, J. Mater. Chem. A 9 (26) (2021) 14841–14850, https://doi.org/10.1039/D1TA01325D.
[7] G. Palani, R. Apsari, M.M. Hanafiah, K. Venkateswarlu, S.K. Lakkaboyana, K. Kannan, A.T. Shivanna, A.M. Idris, C.H. Yadav, Metal-doped graphitic carbon nitride nanomaterials for photocatalytic environmental applications—a review, Nanomater. 12 (10) (2022) 1754.
[8] Y. Xia, H. Yang, W. Ho, B. Zhu, J. Yu, Promoting the photocatalytic NO oxidation activity of hierarchical porous g-C_3N_4 by introduction of nitrogen vacancies and charge channels, Appl. Catal. B: Environ. Energy 344 (2024) 123604, https://doi.org/10.1016/j.apcatb.2023.123604.
[9] S.R. Nagella, R. Vijitha, B. Ramesh Naidu, K.S.V. Krishna Rao, C.-S. Ha, K. Venkateswarlu, Benchmarking recent advances in hydrogen production using g-C_3N_4-based photocatalysts, Nano Energy 111 (2023) 108402, https://doi.org/10.1016/j.nanoen.2023.108402.
[10] A. Murugan, R. Selvaraj Mohana, Environment friendly g-C_3N_4-based catalysts and their recent strategy in organic transformations, High Energy Chem. 56 (2) (2022) 73–90, https://doi.org/10.1134/S0018143922020102.
[11] Y. Wu, F. Li, J. Xue, Z. Lv, Effect of various g-C_3N_4 precursors on the catalytic performance of alkylorganotin-based catalysts in acetylene hydrochlorination, Turk. J. Chem. 44 (2) (2020) 393–408, https://doi.org/10.3906/kim-1909-64.
[12] Z. Lin, S. Wang, Y. Miao, J. Yuan, Y. Liu, S. Xu, S. Cao, One-step preparation of halogenated aminobenzonitrile modified g-C_3N_4 via copolymerization and in situ halogen doping for highly enhanced visible light hydrogen evolution, Int. J. Hydrogen Energy 45 (11) (2020) 6341–6351, https://doi.org/10.1016/j.ijhydene.2019.12.123.
[13] T.R. Pisanic, J.D. Blackwell, V.I. Shubayev, R.R. Fiñones, S. Jin, Nanotoxicity of iron oxide nanoparticle internalization in growing neurons, Biomaterials 28 (2007) 2572–2581.

[14] V. Tripathi, P. Linga Reddy, P.E. Hande, D.S. Vishwakarma, D.J. Fartade, L.S. Panchakarla, S.J. Gharpure, Cobalt nickel bimetallic nanocatalyst supported on g-C_3N_4 for selective hydrogenation of α,β-unsaturated carbonyls and nitroarenes, ChemCatChem (2023) e202300460, https://doi.org/10.1002/cctc.202300460 n/a(n/a).

[15] N. Vahedi-Notash, M.M. Heravi, A. Alhampour, P. Mohammadi, Ag nanoparticles immobilized on new mesoporous triazine-based carbon (MTC) as green and recoverable catalyst for reduction of nitroaromatic in aqueous media, Sci. Rep. 10 (1) (2020) 19322, https://doi.org/10.1038/s41598-020-74232-4.

[16] H. Yang, G. Li, G. Jiang, Z. Zhang, Z. Hao, Heterogeneous selective oxidation over supported metal catalysts: from nanoparticles to single atoms, Appl. Catal. B Environ. 325 (2023) 122384, https://doi.org/10.1016/j.apcatb.2023.122384.

[17] A. Ayati, A. Ahmadpour, F.F. Bamoharram, M.M. Heravi, H. Rashidi, Photocatalytic synthesis of gold nanoparticles using preyssler acid and their photocatalytic activity, Chin. J. Catal. 32 (6) (2011) 978–982, https://doi.org/10.1016/S1872-2067(10)60221-5.

[18] L. Shaker Ardakani, A. Surendar, L. Thangavelu, T. Mandal, Silver nanoparticles (Ag NPs) as catalyst in chemical reactions, Synth. Commun. 51 (10) (2021) 1516–1536, https://doi.org/10.1080/00397911.2021.1894450.

[19] S. Sankar Sana, R. Haldhar, J. Parameswaranpillai, M. Chavali, S.-C. Kim, Silver nanoparticles-based composite for dye removal: a comprehensive review, Clean. Mater. 6 (2022) 100161, https://doi.org/10.1016/j.clema.2022.100161.

[20] X.-T. Yi, T. Zhao, F. Wang, J. Xu, B. Xue, Palladium nanoparticles supported on exfoliated g-C_3N_4 as efficient catalysts for selective oxidation of benzyl alcohol by molecular oxygen, New J. Chem. 45 (30) (2021) 13519–13528, https://doi.org/10.1039/D1NJ01889B.

[21] S. Huang, Y. Zhao, R. Tang, Facile fabrication of a Cu@g-C_3N_4 nanocatalyst and its application for the aerobic oxidations of alkylaromatics and the reduction of 4-nitrophenol, RSC Adv. 6 (93) (2016) 90887–90896, https://doi.org/10.1039/C6RA18288G.

[22] T. Narkbuakaew, V. Intasanta, Modified g-C_3N_4 with boron doping for efficient simultaneous catalytic reduction of Ag^+ and organic pollutants, Mater. Today Sustain. 20 (2022) 100258, https://doi.org/10.1016/j.mtsust.2022.100258.

[23] J. Yang, H. Song, J. Wu, X. Zhu, Ag nanoparticle-modified P-doped tubular g-C_3N_4 for enhanced degradation of organic pollutants, Inorg. Chem. Commun. 153 (2023) 110827, https://doi.org/10.1016/j.inoche.2023.110827.

[24] A. Balakrishnan, M. Chinthala, Comprehensive review on advanced reusability of g-C_3N_4 based photocatalysts for the removal of organic pollutants, Chemosphere 297 (2022) 134190, https://doi.org/10.1016/j.chemosphere.2022.134190.

[25] G. Rahimzadeh, M. Tajbakhsh, M. Daraie, A. Ayati, Heteropolyacid coupled with cyanoguanidine decorated magnetic chitosan as an efficient catalyst for the synthesis of pyranochromene derivatives, Sci. Rep. 12 (1) (2022) 17027, https://doi.org/10.1038/s41598-022-21196-2.

[26] S. Balgude, S. Godase, A. Shinde, C. Harak, Succinate assisted synthesis of magnetically separable Fe_2O_3/g-C_3N_4 nano-heterostructure: a stable catalyst for environmental remediation, Curr. Res. Green Sustain. Chem. 4 (2021) 100210, https://doi.org/10.1016/j.crgsc.2021.100210.

[27] A. Shahinpour, B. Tanhaei, A. Ayati, H. Beiki, M. Sillanpää, Binary dyes adsorption onto novel designed magnetic clay-biopolymer hydrogel involves characterization and adsorption performance: kinetic, equilibrium, thermodynamic, and adsorption mechanism, J. Mol. Liq. 366 (2022) 120303, https://doi.org/10.1016/j.molliq.2022.120303.

[28] S. Hemmati, M.M. Heravi, B. Karmakar, H. Veisi, In situ decoration of Au NPs over polydopamine encapsulated GO/Fe_3O_4 nanoparticles as a recyclable nanocatalyst for the reduction of nitroarenes, Sci. Rep. 11 (1) (2021) 12362, https://doi.org/10.1038/s41598-021-90514-x.

[29] K.J. Datta, A.K. Rathi, P. Kumar, J. Kaslik, I. Medrik, V. Ranc, R.S. Varma, R. Zboril, M.B. Gawande, Synthesis of flower-like magnetite nanoassembly: application in the efficient reduction of nitroarenes, Sci. Rep. 7 (1) (2017) 11585, https://doi.org/10.1038/s41598-017-09477-7.

[30] P. Mohammadi, M. Heravi, M. Daraie, Ag nanoparticles immobilized on new magnetic alginate halloysite as a recoverable catalyst for reduction of nitroaromatics in aqueous media, Sci. Rep. 11 (1) (2021) 17124, https://doi.org/10.1038/s41598-021-96421-5.

[31] A. Ayati, B. Tanhaei, F.F. Bamoharram, A. Ahmadpour, P. Maydannik, M. Sillanpää, Photocatalytic degradation of nitrobenzene by gold nanoparticles decorated polyoxometalate immobilized TiO2 nanotubes, Sep. Purif. Technol. 171 (2016) 62–68, https://doi.org/10.1016/j.seppur.2016.07.015.

[32] X. Qiu, Q. Liu, M. Song, C. Huang, Hydrogenation of nitroarenes into aromatic amines over Ag@BCN colloidal catalysts, J. Colloid Interface Sci. 477 (2016) 131–137, https://doi.org/10.1016/j.jcis.2016.05.043.

[33] M. Piri, M.M. Heravi, A. Elhampour, F. Nemati, Silver nanoparticles supported on P, Se-codoped g-C_3N_4 nanosheet as a novel heterogeneous catalyst for reduction of nitroaromatics to their corresponding amines, J. Mol. Struct. 1242 (2021) 130646, https://doi.org/10.1016/j.molstruc.2021.130646.

[34] D. Huang, G. Yan, Recent advances in reactions of azides, Adv. Synth. Catal. 359 (10) (2017) 1600–1619, https://doi.org/10.1002/adsc.201700103.

[35] Z. Chen, Z. Liu, G. Cao, H. Li, H. Ren, Recent advances in multicomponent synthesis of 1,4,5-trisubstituted 1,2,3-triazoles, Adv. Synth. Catal. 359 (2) (2017) 202–224, https://doi.org/10.1002/adsc.201600918.

[36] S. Payra, A. Saha, S. Banerjee, On water Cu@g-C_3N_4 catalyzed synthesis of NH-1,2,3-Triazoles via [2+3] cycloadditions of nitroolefins/alkynes and sodium azide, ChemCatChem 10 (23) (2018) 5468–5474, https://doi.org/10.1002/cctc.201801524.

[37] Y.H. Lau, P.J. Rutledge, M. Watkinson, M.H. Todd, Chemical sensors that incorporate click-derived triazoles, Chem. Soc. Rev. 40 (5) (2011) 2848–2866, https://doi.org/10.1039/C0CS00143K.

[38] A. Yadav, C.P. Kaushik, M. Kumar, Hydrazones tethered disubstituted 1,2,3-triazoles: design, synthesis, antitubercular and antimicrobial evaluation, J. Mol. Struct. 1283 (2023) 135163, https://doi.org/10.1016/j.molstruc.2023.135163.

[39] D. Addla, A. Jallapally, D. Gurram, P. Yogeeswari, D. Sriram, S. Kantevari, Rational design, synthesis and antitubercular evaluation of novel 2-(trifluoromethyl) phenothiazine-[1,2,3]triazole hybrids, Bioorg. Med. Chem. Lett. 24 (1) (2014) 233–236, https://doi.org/10.1016/j.bmcl.2013.11.031.

[40] K.D. Thomas, A.V. Adhikari, N.S. Shetty, Design, synthesis and antimicrobial activities of some new quinoline derivatives carrying 1,2,3-triazole moiety, Eur. J. Med. Chem. 45 (9) (2010) 3803–3810, https://doi.org/10.1016/j.ejmech.2010.05.030.

[41] K. Kushwaha, N. Kaushik, Lata, S.C. Jain, Design and synthesis of novel 2H-chromen-2-one derivatives bearing 1,2,3-triazole moiety as lead antimicrobials, Bioorg. Med. Chem. Lett. 24 (7) (2014) 1795–1801, https://doi.org/10.1016/j.bmcl.2014.02.027.

[42] R. Alvarez, S. Velazquez, A. San-Felix, S. Aquaro, E.D. Clercq, C.-F. Perno, A. Karlsson, J. Balzarini, M.J. Camarasa, 1,2,3-Triazole-[2,5-Bis-O-(tert-butyldimethylsilyl)-.beta.-D-ribofuranosyl]-3'-spiro-5''-(4''-amino-1'',2''-oxathiole 2'',2''-dioxide) (TSAO) Analogs, Synthesis and anti-HIV-1 activity, J. Med. Chem. 37 (24) (1994) 4185–4194, https://doi.org/10.1021/jm00050a015.

[43] R.S. Bohacek, C. McMartin, W.C. Guida, The art and practice of structure-based drug design: a molecular modeling perspective, Med. Res. Rev. 16 (1) (1996) 2–6, https://doi.org/10.1002/(SICI)1098-1128(199601)16:1<3::AID-MED1>3.0.CO, 3-50.

[44] P.W. Szafrański, A. Siwek, I. Smaga-Maślanka, L. Pomierny-Chamioło, P. Ilnicki, G. Żuchowski, T. Nevalainen, M. Filip, P. Zajdel, M.T. Cegła, Synthesis, relative configuration and CB1 receptor affinity studies for a set of 1,2,3-triazole derivatives, J. Mol. Struct. 1282 (2023) 135223, https://doi.org/10.1016/j.molstruc.2023.135223.

[45] S.K. Verma, R. Verma, Y.R. Girish, S. Verma, K. Pramoda, Y. Vaishnav, J. Saji, K.S.S. Kumar, Two-dimensional Ti_3C_2Tx MXenes as a catalyst support for the synthesis of 1,4-disubstituted-1,2,3-triazoles via azide-nitroalkene oxidative cycloaddition, J. Mol. Struct. (2023), https://doi.org/10.1016/j.molstruc.2023.135145, 1281: 135145.

[46] G.D. Saratale, R.G. Saratale, S.-K. Cho, G. Ghodake, R.N. Bharagava, Y. Park, S.I. Mulla, D.-S. Kim, A. Kadam, S. Nair, H.-S. Shin, Investigation of photocatalytic degradation of reactive textile dyes by Portulaca oleracea-functionalized silver nanocomposites and exploration of their antibacterial and antidiabetic potentials, J. Alloys Compd. 833 (2020) 155083, https://doi.org/10.1016/j.jallcom.2020.155083.

[47] A.Z. Moghaddam, E. Ghiamati, A. Ayati, M.R. Ganjali, Application of the response surface methodology (RSM) for optimizing the adsorptive removal of chromate using a magnetic cross-linked chitosan nanocomposite, J. Appl. Polym. Sci. 136 (2019) 47077, https://doi.org/10.1002/app.47077.

[48] B. Tanhaei, A. Ayati, F.F. Bamoharram, M. Sillanpää, Magnetic EDTA functionalized Preyssler cross linked chitosan nanocomposite for adsorptive removal of Pb (II) ions. Clean, Air, Soil, Water 45 (10) (2017), https://doi.org/10.1002/clen.201700328.

[49] P. Mohammadi, M.M. Heravi, S. Sadjadi, Green synthesis of Ag NPs on magnetic polyallylamine decorated g-C_3N_4 by Heracleum persicum extract: efficient catalyst for reduction of dyes, Sci. Rep. 10 (1) (2020) 6579, https://doi.org/10.1038/s41598-020-63756-4.

[50] R.J. Mudakavi, S. Vanamali, D. Chakravortty, A.M. Raichur, Development of arginine based nanocarriers for targeting and treatment of intracellular Salmonella, RSC Adv. 7 (12) (2017) 7022–7032, https://doi.org/10.1039/C6RA27868J.

[51] B. Tanhaei, A. Ayati, E. Iakovleva, M. Sillanpää, Efficient carbon interlayed magnetic chitosan adsorbent for anionic dye removal: synthesis, characterization and adsorption study, Int. J. Biol. Macromol. 164 (2020) 3621–3631, https://doi.org/10.1016/j.ijbiomac.2020.08.207.
[52] S. Wunder, F. Polzer, Y. Lu, Y. Mei, M. Ballauff, Kinetic analysis of catalytic reduction of 4-nitrophenol by metallic nanoparticles immobilized in spherical polyelectrolyte brushes, J. Phys. Chem. C 114 (19) (2010) 8814–8820, https://doi.org/10.1021/jp101125j.
[53] S. Das, S. Jana, A facile approach to fabricate halloysite/metal nanocomposites with preformed and in situ synthesized metal nanoparticles: a comparative study of their enhanced catalytic activity, Dalton Trans. 44 (19) (2015) 8906–8916, https://doi.org/10.1039/C5DT00830A.
[54] M. Daraie, M.M. Heravi, P. Mohammadi, A. Daraie, Silver incorporated into g-C_3N_4/Alginate as an efficient and heterogeneous catalyst for promoting click and A3 and KA2 coupling reaction, Sci. Rep. 11 (1) (2021) 14086, https://doi.org/10.1038/s41598-021-93239-z.
[55] M. Daraie, M.M. Heravi, A biocompatible chitosan-ionic liquid hybrid catalyst for regioselective synthesis of 1,2,3-triazols, Int. J. Biol. Macromol. 140 (2019) 939–948, https://doi.org/10.1016/j.ijbiomac.2019.08.162.
[56] T. Hossiennejad, M. Daraie, M.M. Heravi, N.N. Tajoddin, Computational and experimental investigation of immobilization of CuI nanoparticles on 3-amino-pyridine modified poly(styrene-co-maleic anhydride) and its catalytic application in regioselective synthesis of 1,2,3-triazoles, J. Inorg. Organomet. Polym. Mater. 27 (4) (2017) 861–870, https://doi.org/10.1007/s10904-017-0530-z.
[57] E. Hashemi, Y.S. Beheshtiha, S. Ahmadi, M.M. Heravi, In situ prepared CuI nanoparticles on modified poly(styrene-co-maleic anhydride): an efficient and recyclable catalyst for the azide-alkyne click reaction in water, Trans. Met. Chem. 39 (5) (2014) 593–601.